International Journal of Nanomedicine

Dovepress
open access to scientific and medical research

Open Access Full Text Article

ORIGINAL RESEARCH

Nasal Absorption Enhancement of Mometasone Furoate Nanocrystal Dispersions

Shuya Masuda[1]*, Saori Deguchi[1]*, Fumihiko Ogata[1], Joji Yoshitomi[1], Hiroko Otake[1], Kazutaka Kanai[2], Naohito Kawasaki[1], Noriaki Nagai[1]

[1]Faculty of Pharmacy, Kindai University, Osaka, Japan; [2]Department of Small Animal Internal Medicine, School of Veterinary Medicine, University of Kitasato, Aomori, Japan

*These authors contributed equally to this work

Correspondence: Noriaki Nagai, Faculty of Pharmacy, Kindai University, 3-4-1 Kowakae, Higashi-Osaka, Osaka, 577-8502, Japan, Tel +81 6 4307 3638, Fax +81 6 6730 1394, Email nagai_n@phar.kindai.ac.jp

Purpose: We designed a 0.05% mometasone furoate (MF) nanocrystal dispersion and investigated whether the application of MF nanocrystals in nasal formulations enhanced local absorption compared to traditional nasal MF formulations (CA-MF).

Methods: MF nanocrystal dispersions (MF-NPs) were prepared by bead milling MF microcrystal dispersions (MF-MPs) consisting of MF, 2-hydroxypropyl-β-cyclodextrin, methylcellulose, and purified water. Pluronic F-127 combined with methylcellulose, Pluronic F-68, or carbopol was used as a base for in situ gelation (thickener). MF concentrations were measured using high-performance liquid chromatography, and nasal absorption of MF was evaluated in 6 week-old male Institute of Cancer Research (ICR) mice.

Results: The particle size range of MF prepared with the bead mill treatment was 80–200 nm, and the nanoparticles increased the local absorption of MF, which was higher than that of CA-MF and MF-MPs. In addition, unlike the results obtained in the small intestine and corneal tissue, the high absorption of nanocrystalline MF in the nasal mucosa was related to a pathway that was not derived from energy-dependent endocytosis. Moreover, the application of the in situ gelling system attenuated the local absorption of MF-NPs, owing to a decrease in drug diffusion in the dispersions.

Conclusion: We found that nanoparticulation of MF enhances local intranasal absorption, and nasal bioavailability is higher than that of CA-MF. In addition, we demonstrate that viscosity regulation is an important factor in the design of nasal formulations based on MF nanocrystals. These findings provide insights for the design of novel nanomedicines with enhanced nasal bioavailability.

Plain Language Summary: Mometasone furoate (MF) is administered nasally to treat nasal inflammatory diseases. In this study, we designed MF nanocrystal dispersions (MF-NPs) and investigated whether the application of MF nanocrystals in nasal MF formulations enhanced local absorption compared to traditional nasal MF formulations. MF-NPs were obtained via bead-milling of dispersions, consisting of MF, 2-hydroxypropyl-β-cyclodextrin, methylcellulose, and purified water, and the MF-NPs with in situ gelation were prepared by the addition of a gel base consisting of Pluronic F-127 combined with methylcellulose, Pluronic F-68, or carbopol. The nasal absorption of MF was evaluated in 6 week-old ICR mice. The bead-milled MF particles in the dispersions were crystalline with sizes of 80–200 nm. Moreover, MF-NPs exhibited lower viscosity and higher local absorption than commercially available nasal formulations and dispersions containing microcrystalline MF. However, the application of in situ gelling systems attenuated the local absorption of the MF-NPs. This is the first study to investigate the nasal absorption of dispersions containing nanocrystalline MF and the basis of in situ gelation, providing important information for the design of nanomedicines with enhanced nasal bioavailability.

Keywords: mometasone furoate, nanocrystal, nasal absorption, drug delivery, in situ gel

Introduction

The prevalence of allergic rhinitis and rhinosinusitis has increased over the past decade.[1–3] Currently recommended drug therapies for rhinitis and rhinosinusitis consist primarily of nasal corticosteroids, antihistamines, and oral and nasal

Received: 19 July 2023
Accepted: 5 October 2023
Published: 9 October 2023

Graphical Abstract

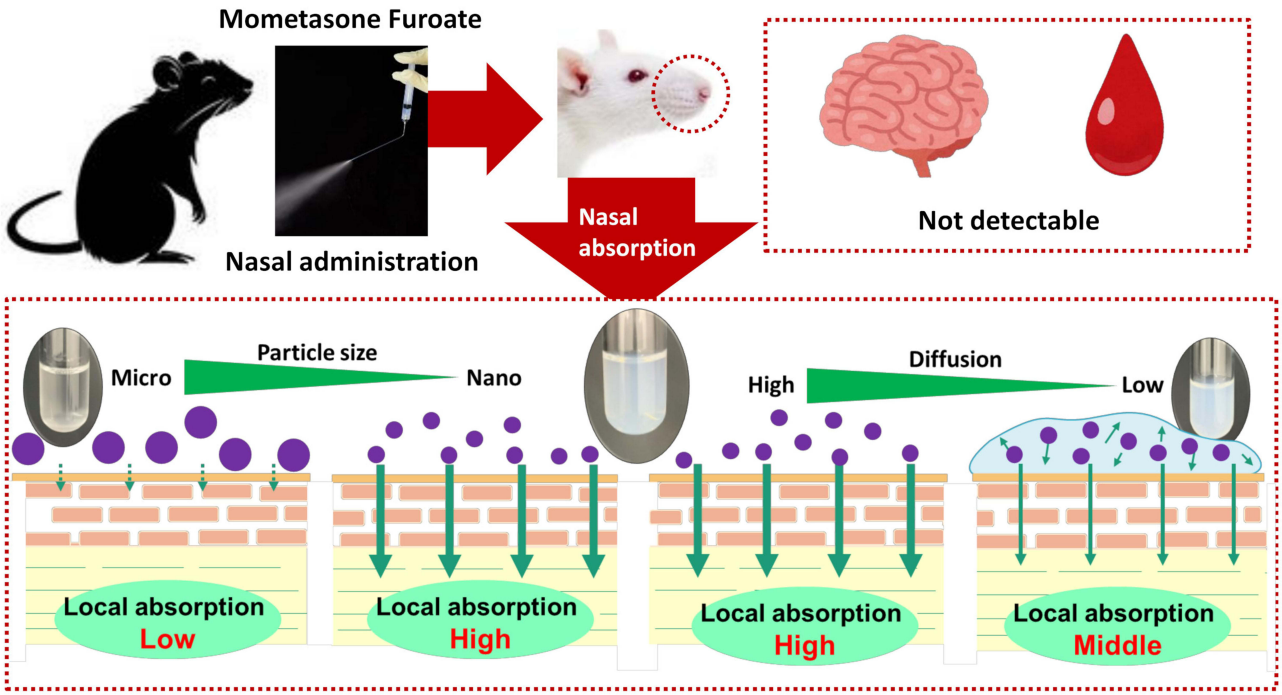

decongestants. Nasal corticosteroids are used as first-line agents, especially in patients with perennial or moderate-to-severe symptoms, or when nasal obstruction is a major problem.[4–7]

Mometasone furoate (MF), a white powder with a molecular weight of 539.45, is a corticosteroid that is used to treat rhinitis and rhinosinusitis. MF inhibits the arachidonic acid pathway, significantly suppressing the production of leukotrienes, inflammatory cytokines, and growth factors, and the expression of adhesion molecules.[8] MF is a lipophilic compound with low water solubility developed for topical administration,[9] and the absorbed drug is mainly excreted in bile as a metabolite and less frequently in urine.[9] In clinical settings, a nasal formulation of MF is commercially available as NASONEX nasal 50 µg/spray (traditional nasal MF formulations, CA-MF), a metered-dose pump spray with a pH of 4.3–4.9.

Drugs administered through the nose are absorbed and exert both local and systemic effects. During this process, the mucosal layer, epithelial cell membranes, and capillary endothelium in the nasal cavity act as barriers to drug absorption in the bloodstream. In addition, nasal mucociliary clearance is the primary innate defense mechanism of the nose and paranasal sinuses, and epithelial cilia beat in a coordinated and unidirectional fashion to transport mucus from the epithelium to various drainage sites, thus removing inhaled particles and irritants under normal conditions.[10] The nasal cavity has a thin mucus layer, which is more easily accessible and permeable than other mucosal surfaces.[11] The epithelial cell membrane is composed of layers of pseudostratified columnar cells interconnected via tight junctions, and small hydrophobic molecules can pass through the biomembrane via concentration gradients. Hydrophilic molecules require selective transport systems to pass through lipid bilayers. Large polar drugs are absorbed by paracellular mechanisms, and tight junction structures provide a barrier to this absorption. Once a drug molecule passes through the basolateral side of the epithelium, the capillary endothelium in the blood acts as a barrier. Thus, drug absorption from the nasal respiratory epithelium is mediated by transcellular, paracellular, carrier-mediated transport, and transcytosis mechanisms.[12] Furthermore, when drugs are administered into the nasal cavity, they reach the nasal mucosa and are directly transmitted to the brain via the olfactory pathway. Drugs pass through the olfactory epithelium, enter the perineuronal cavity via paracellular mechanisms, and migrate directly into the brain.[13]

Protease inhibitors, in situ gelling agents, thickeners, tight junction modulators, cationic polymers, cyclodextrins, and surfactants can enhance nasal absorption. Nanotechnology-based drug delivery can be used to overcome the chemical, physiological, anatomical, and clinical barriers associated with conventional drugs. Many types of nanotherapeutics, such as those based on micelles, polymers, and liposomes as carrier materials, have been developed.[14] The potential advantages of nanocrystal formulation include improved drug stability and solubility, increased bioavailability at the targeted area, and prolonged duration of action via controlled release. We have previously reported that nanodispersions containing fluorometholone, minoxidil, and indomethacin exhibited improved solubility and membrane permeability.[15–18] Nanodispersions may also enhance nasal bioavailability and may be used as nasal delivery systems for MF. In this study, we designed MF nanocrystal dispersions (MF-NPs), and investigated whether their application in nasal formulations enhanced local absorption compared to traditional nasal MF formulations.

Materials and Methods

Animals

All animal experiments were performed in accordance with the guidelines of the Kindai University and the Japanese Pharmacological Society. Six-week-old male Institute of Cancer Research (ICR) mice (n=277 mice, approximately 31.1 g) were provided by Clea Japan, Inc. (Tokyo, Japan) and housed at 25°C. Water and CE-2 standard diet (Clare Japan, Tokyo, Japan) were provided ad libitum. In this study, mice were anaesthetized with isoflurane (3%, flow rate 1 L/min). Euthanasia was performed by injecting pentobarbital (200 mg/kg, i.p.) according to the AVMA guidelines 2020, and was approved by Kindai University on April 1, 2020, with project identification code KAPS-2020-013. This study was conducted in accordance with the ARRIVE guidelines.

Chemicals

MF powder and NASONEX® Nasal 50 μg (CA-MF) were provided from Tokyo Chemical Industry Co., Ltd (Tokyo, Japan), KYORIN Pharmaceutical Co., Ltd. (Tokyo, Japan), respectively. Isoflurane, Pluronic F-68, cytochalasin D, and butyl p-hydroxybenzoate were purchased from Wako Pure Chemical Industries, Ltd. (Osaka, Japan). Two-hydroxypropyl -β-cyclodextrin (HPβCD) and Bio-Rad Protein Assay Kit were purchased from Nihon Shokuhin Kako Co., Ltd. (Tokyo, Japan) and Bio-Rad (CA, USA), respectively. Dynasore and rottlerin were obtained from Nacalai Tesque (Kyoto, Japan) and nystatin was obtained from Sigma-Aldrich (St. Louis, MO, USA). Pluronic F-127 was purchased from Funakoshi Co., Ltd. (Tokyo, Japan), and methylcellulose (MC) was purchased from Shin-Etsu Chemical Co. Ltd. (Tokyo, Japan). All other chemicals and organic solvents were of analytical grade.

Preparation of MF Micro- and Nanocrystal Dispersions

The dispersions containing MF micro- and nanocrystals were prepared following our previous reports.[15–19] Briefly, MF powder, HPβCD, and MC were suspended in purified water (dispersions containing mometasone furoate microcrystals, MF-MPs). The MF-NPs were prepared by bead milling. The mill treatment was performed using a ShakeMaster®NEO BMS-M10N21 (BioMedical Science, Tokyo, Japan) with 0.1 mm zirconia beads at 1500 rpm for 3 h at 4°C. Nanocrystal dispersions with thickeners (in situ gel formulations) were prepared as follows: Pluronic F-127 combined with MC, Pluronic F-68, or carbopol was added to the MF-NPs as base for in situ gelation, which were used as MF-NPs@F127/MC, MF-NPs@F127/F68, and MF-NPs@F127/Car, respectively. The compositions of the MF dispersions are listed in Table 1. The contents of the additives and pH (4.9) were determined according to our previous studies[20,21] and the pH of the CA-MF, respectively.

Measurement of MF Concentration

MF concentration was measured by high-performance liquid chromatography (HPLC) using an LC-20AT HPLC system (Shimadzu Corp., Kyoto, Japan) (wavelength, 254 nm). Inertsil ODS-3 column (2.1×50 mm, GL Science Co., Inc., Tokyo, Japan) was selected, column temperature was set at 35°C. The mobile phase (methanol/purified water/acetonitrile, 50/43/7) were followed at 250 μL. The sample was mixed with a butyl p-hydroxybenzoate (1 μg/mL, internal standard)

Table 1 Compositions of Mometasone Furoate (MF) Formulations Used in This Study

Formulation	Content (w/v %)						
	MF	HPβCD	MC	Pluronic F-127	Pluronic F-68	Carbopol	
MF-MPs	0.05	5	0.5	-	-	-	-
MF-NPs	0.05	5	0.5	-	-	-	Bead mill
MF-NPs@F127/MC	0.05	5	1.5	7	-	-	Bead mill
MF-NPs@F127/F68	0.05	5	0.5	7	1.5	-	Bead mill
MF-NPs@F127/Car	0.05	5	0.5	7	-	0.15	Bead mill

Note: Data are expressed as w/v%.

in methanol, and 10 μL of the mixture was injected into the HPLC system. The internal standard and MF of retention time was 5.1 min and 16.8 min, respectively and the subsequent favorable calibration curve was $y = 0.239x + 0.0076$ ($R^2 = 0.9986$). The lower limit of quantification was 0.57 μM.

Particle Size of MF in Dispersions

A laser diffraction particle size analyzer, SALD-7100 (Shimadzu Corp.), was used to measure the MF particles in CA-MF and MF-MPs, and the refractive index was set at 1.60–0.010i. In addition, the particle distribution of dispersions containing MF nanocrystals with or without the thickener was determined using dynamic light scattering NANOSIGHT LM10 (QuantumDesign Japan, Tokyo, Japan) at a viscosity of 1.45 mPa·s, wavelength of 405 nm, and measurement time of 60s. Moreover, the phase and height images of MF-NFs with or without the thickener were obtained using Scanning Probe Microscope (SPM)-9700 (Shimadzu Corp.), and these images were combined and expressed as SPM images.

Solubility of MF in Dispersions

The solubilized and non-solubilized MF in MF-NPs with or without a thickener were separated and centrifuged at $1\times10^5 \times g$ using a Beckman Optima™ MAX-XP Ultracentrifuge (Beckman Coulter, Osaka, Japan). Subsequently, the concentration of solubilized MF was measured using the HPLC method described above and expressed as the solubility of MF in the dispersions.

Membrane Permeability of MF in Dispersions

The membrane permeability of MF was evaluated according to our previous reports using Franz diffusion cell.[18] Briefly, 12.2 mL of 0.2 mM phosphate buffer (pH 7.2) were filled in the reservoir chamber of Franz diffusion cell, and a 0.45 μm pore-size membrane filters (MF™-MEMBRANE FILTER, Merck Millipore, Tokyo, Japan) was fixed on the cell. After that, 200 μL of MF dispersions with or without thickener were added to the 0.45 μm membrane filter (2 cm^2), and incubated at 37°C for 5 min. Then, two hundred microliters of phosphate buffer were withdrawn from the reservoir chamber, the MF concentration was measured by HPLC method described above. In the experiments using dispersions containing nanocrystalline MF, membrane permeability was expressed as drug diffusion in the dispersions.

Viscosity of MF Dispersions

The four milliliters of MF dispersions with or without thickener were set to a CPZ-52Z plate in Brookfield digital viscometer (Brookfield Engineering Laboratories, Inc., Middleboro, MA, USA), and measured the viscosity at 60 rpm (rotational speed) for 3.5 min under 20–40°C conditions. During the measurement, the pH of the MF-NPs@in situ gel was regulated to simulate that of the nasal cavity (pH 7.2) using NaOH.

Zeta Potential of MF in Dispersions

The ten milliliters of MF dispersions with or without thickener were set to a Zeta Potential Meter Model 502 (Nihon Rufuto Co., Ltd., Tokyo, Japan), and the zeta potential were measured at 49 V, 25°C condition.

Dispersibility of MF Dispersions

The experiment was performed as described in our previous reports.[20,21] First, three microliters of each MF dispersion were incubated in 5 mL test tubes in the dark at 20°C for 2 weeks, and images of the dispersions were captured with a digital camera. Moreover, the fifty microliters of MF dispersions were withdrawn from 5 mm under the surface, and the MF concentration was measured by the HPLC methods described above. The dispersibility of the MF dispersions was determined by measuring the difference in MF concentrations before and after the start of the experiment.

Powder X-Ray Diffraction (XRD)

The crystalline forms of MF in the MF-MPs and MF-NPs were measured using an XRD analyzer Mini Flex II (Rigaku Co., Tokyo, Japan) at a scanning rate, 10°/min; diffraction angles of 5°–90°; X-rays at 30 kV and 15 mA. Dried samples were obtained by volatilizing the dispersion solvent using a TAITEC VC-15SP CENTRIFUGAL CONCENTRATOR (Aich, Japan), and 100 mg of the powder was analyzed using an XRD analyzer Mini Flex II XRD analyzer to measure the crystalline form.

Thermogravimetry-Differential Thermal Analysis (TG-DTA)

The solvents of the MF-MPs and MF-NPs were volatilized using a TAITEC VC-15SP CENTRIFUGAL CONCENTRATOR, and five milligrams of the powder was set using the simultaneous TG-DTA apparatus DTG-60H (Shimadzu Corp.), and the TG-DTA patterns (melting point) were detected under a nitrogen atmosphere. The temperature was maintained at 5°C /min.

Nasal Absorption of MF Dispersions

MF dispersions with or without thickener (2 μL) were nasally administered to ICR mice, and the mice were euthanized by injecting a lethal dose of pentobarbital (200 mg/kg), and the blood was collected from vena cava 0.5, 1, 3, and 5 h after nasal administration. The nasal mucosa and brain were removed by dissecting scissors and scalpels at the same time as above; 0.5, 1, 3, and 5 h after nasal administration, respectively. The nasal mucosa and brain were homogenized with 150 μL of methanol, homogenates and collected blood were centrifuged at 800 × g for 15 min at 4°C, and the supernatant was used for measurement. MF concentrations in the collected samples were measured using HPLC as described above. MF levels in the tissues were expressed as nmol/mg protein and proteins were measured using a Bio-Rad Protein Assay Kit. In addition, the area under the drug concentration–time curve ($AUC_{0\text{-}5h}$) in the nasal mucosa was analyzed using the trapezoidal rule.

In this study, nystatin (54 μM),[22] dynasore (40 μM),[23] rottlerin (2 μM),[24] and cytochalasin D (10 μM)[22] were selected as inhibitors of caveolae-dependent endocytosis (CavME), clathrin-dependent endocytosis (CME), macropinocytosis (MP), and phagocytosis, respectively, and the energy-dependent endocytosis was inhibited using these four pharmacological inhibitors. Pharmacological inhibitors were dissolved in HEPES buffer containing 0.5% dimethyl sulfoxide (DMSO, control). Two microliters of pharmacological inhibitors were nasally administered to mice 30 min before administration of the MF formulation.

In total, 277 mice were used in this study. The above experimental conditions were grouped into eleven groups: CA-MF (n = 28), MF-MPs (n = 32), MF-NPs (n = 40), MF-NPs@F127/MC (n = 24), MF-NPs@F127/F68 (n = 24), MF-NPs @F127/Car (n = 24), combination of MF-NPs and vehicle (control, n=20), nystatin (n = 20), dynasore (n = 20), rottlerin (n = 20), or cytochalasin D (n = 20). Five untreated mice were used for measurement at 0 h.

Statistical Analysis

The JMP ver. 5.1 (SAS Institute) was used for the statistical analysis. One-way analysis of variance (ANOVA) followed by the Tukey–Kramer test was used for statistical analysis. The data are expressed as mean ± standard error (S.E.) of the mean, and the sample numbers (n) are shown in Figure legends.

Results

Evaluation of the Characteristics of MF-NP Dispersions

Figure 1 shows the changes in the particle size distribution of MF with and without bead milling. The particles of CA-MF ranged in size from 0.2 μm to 100 μm. The particle size distribution of the MF-MPs was also observed at a microscale. In contrast, the mean particle size of MF-NPs was 148.9 ± 2.4 nm. Figure 2 shows the XRD peak patterns and TG-DTA curves of MF in the MF-MPs and MF-NPs. The XRD peak patterns of MF in the MF-NPs were similar to the MF-MPs. It was known that two endothermic peaks between 225–240°C are detected in the DSC thermogram of raw MF showing the melting point of MF.[25] In this study, the two peaks in the DTA analysis were detected at 226.1 and 233.3°C, respectively, in the MF powder. This peak pattern is correlated with the previous DSC data.[25] In addition, no difference was observed between the MF powder and prepared MF formulations (MF-MPs and MF-NPs). Figure 3 shows the changes in the solubility, membrane permeability, and dispersibility of MF with or without bead milling. The solubility was enhanced by the bead-milling treatment, and the solubility of MF in the MF-NPs was 56.4–,15.4–fold of CA-MF and MF-MPs, respectively. The proportion of MF particles in the MF-NPs was only 34.2% in liquid form (solid form: 65.8%). The membrane permeability of MF-NPs was higher than CA-MF and MF-MPs, and the dispersibility of the nanocrystalline MF was significantly higher than microcrystalline MF, as sedimentation in the MF-NPs was more gradual than that in the MF-MPs. Moreover, the dispersibility of the MF in the MF-NPs was similar to that in CA-MF. Based on the dispersibility results, we measured the viscosity and zeta potential, which are known factors that enhance the dispersibility of MF-NPs (Figure 4). Neither viscosity nor zeta potential differed between MF-MPs and MF-NPs; the zeta potential showed a negative charge. Although the zeta potential of CA-MF was also negatively charged, the value of the negative charge was significantly higher than those of MF-MPs and MF-NPs. In addition, the viscosity of CA-MF was 10.3–, 10.1–fold of MF-MPs and MF-NP viscosities, respectively, at 40°C.

Nasal Absorption of MF in Mice Treated with CA-MF, MF-MPs, and MF-NPs

It has been reported that the nose-to-brain pathway is a potential route for the transport of nanocrystals in the recent research.[26] Therefore, we investigated whether MF was detected in the nasal mucosa, brain, and blood. No drug delivery

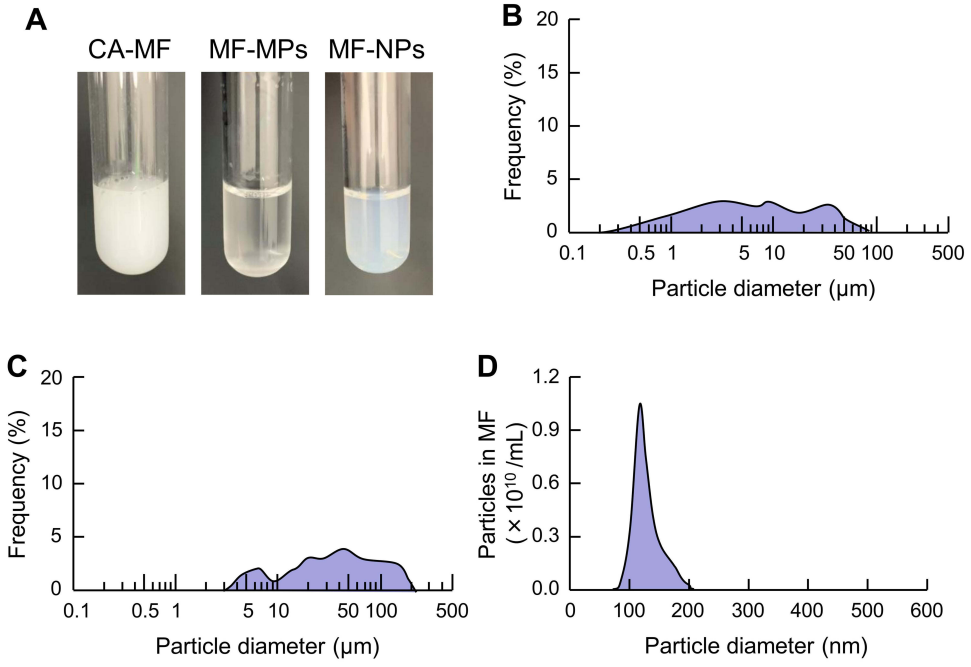

Figure 1 Digital image (**A**) and particle size frequencies of commercially available mometasone furoate (CA-MF) (**B**), MF microcrystal dispersions (MF-MPs) (**C**), and MF nanocrystal dispersions (MF-NPs) (**D**).

Notes: The Compositions of MF formulations are listed in Table 1. The particle distributions shown in (**B** and **C**) were determined using a laser diffraction particle size analyzer (SALD-7100). On the other hand, the data in (**D**) was obtained by dynamic light scattering NANOSIGHT LM10.

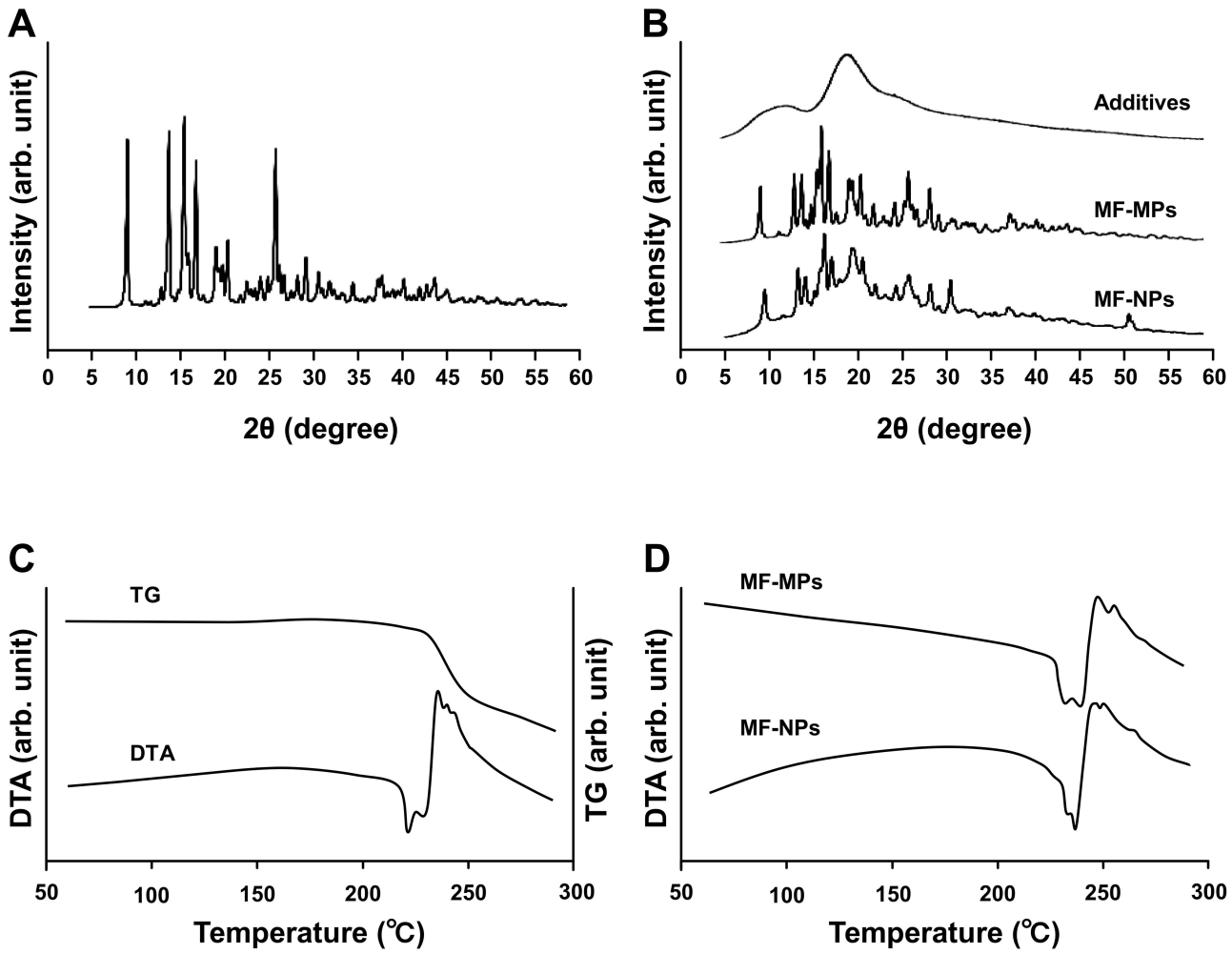

Figure 2 Analysis of the crystal structures of MF in MF-MPs and MF-NPs.
Notes: The Compositions of MF formulations are listed in Table 1. (**A**) X-ray diffraction (XRD) patterns of commercially available MF powders without additives or bead mill treatment. (**B**) XRD patterns of additives, MF-MPs, and MF-NPs. (**C**) Thermogravimetric differential thermal analysis (TG-DTA) curves of commercially available MF powders without additives or bead mill treatments. (**D**) DTA curves of the MF-MPs and MF-NPs.

to the brain or blood was observed 0–5 h after nasal administration of the MF dispersions, as MF levels were below the detection sensitivity in the brain and blood of mice nasally administered CA-MF, MF-MPs, and MF-NPs. In contrast to the results for brain and blood, MF was detected in the nasal mucosa; Figure 5A and B shows the changes in MF content in the nasal mucosa of mice nasally administered CA-MF, MF-MPs, and MF-NPs. The MF content in the nasal mucosa of mice nasally administered NF-NPs was significantly enhanced compared to that in mice nasally administered MF-MPs, and the MF levels of MF-NPs were also higher than those of CA-MF 30 min after nasal administration.

Our previous reports showed that energy-dependent endocytosis is involved in the high absorption of drug nanocrystals.[15–21] Therefore, we also measured whether phagocytosis inhibitors (nystatin, dynasore, rottlerin, and cytochalasin D) prevented the high nasal absorption of MF-NPs (Figure 5C). Contrary to our expectations, the MF content in the nasal mucosa of mice that were nasally administered MF-NPs was not altered by pretreatment with phagocytosis inhibitors.

Effects of Thickener on the Characteristics and Nasal Absorption of MF-NPs

Viscosity is related to drug retention and absorption in the nasal mucosa.[27,28] In this study, we prepared the MF-NPs containing thickener (MF-NPs@F127/MC, MF-NPs@F127/F68, MF-NPs@F127/Car), and evaluated the characteristics and nasal absorption. Figure 6A–E show the particle size distributions of the MF-NPs with thickeners. MF-NPs@F127/

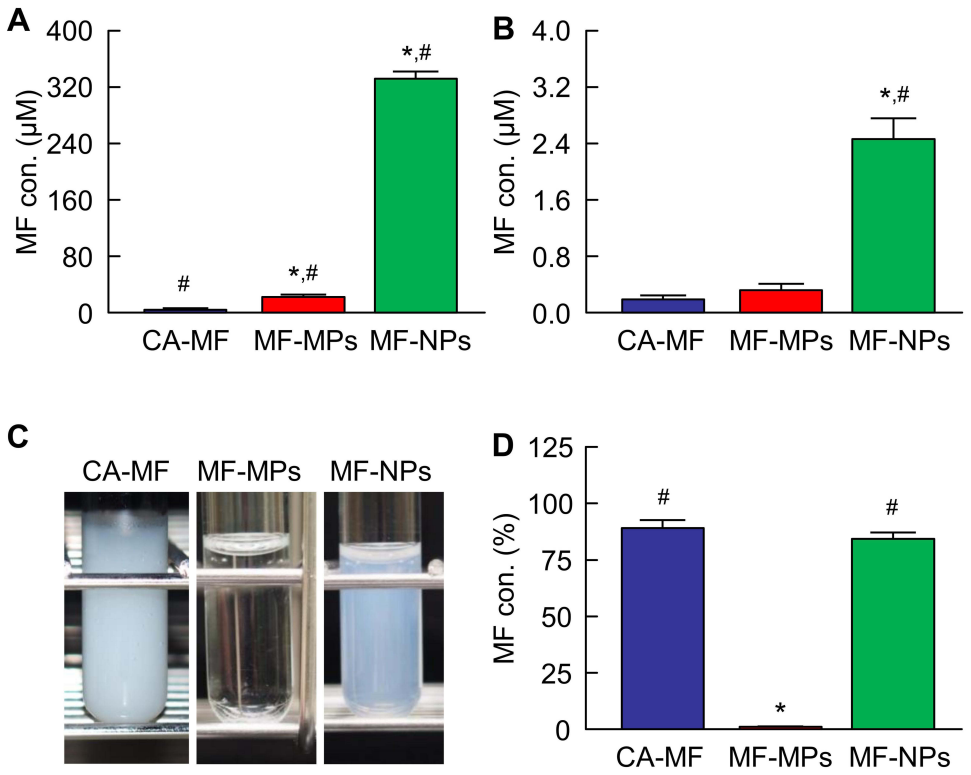

Figure 3 Evaluation of the solubilities (**A**), membrane permeabilities (**B**), and dispersibilities (**C** and **D**) of CA-MF, MF-MPs, and MF-NPs.
Notes: The Compositions of MF formulations are listed in Table 1. (**C**) and (**D**) Photographs (**C**) and dispersibilities (MF concentration in surface/total MF) (**D**) of CA-MF, MF-MPs, and MF-NPs 2 weeks after preparation. n = 7. *P<0.05 vs CA-MF. #P<0.05 vs MF-MPs.

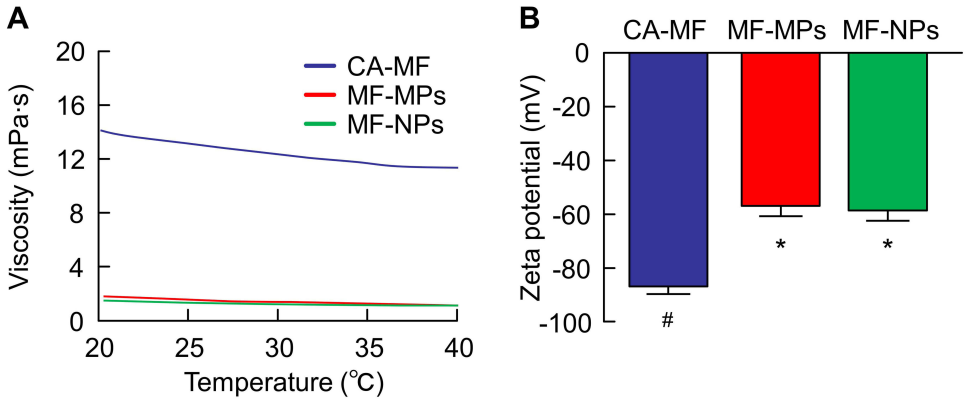

Figure 4 Changes in the viscosities (**A**) and zeta potentials (**B**) of CA-MF, MF-MPs, and MF-NPs.
Notes: The Compositions of MF formulations are listed in Table 1. The viscosity was measured at 20–40 °C. n = 5–7 (viscosity: n=5; zeta potential: n=7). *P<0.05 vs CA-MF. #P<0.05 vs MF-MPs.

MC, MF-NPs@F127/F68, MF-NPs@F127/Car were nanosized with their mean particle size being 153.1 ± 3.1, 150.9 ± 2.8, and 153.5 ± 3.3 nm, respectively (Table 2). Figure 6F shows the changes in viscosity of MF-NPs with thickener at 20–40°C. The addition of a thickener enhanced viscosity, and the viscosities of MF-NPs@F127/MC and MF-NPs@F127/F68 were similar. The viscosity of MF-NPs@F127/Car was higher than those of MF-NPs@F127/MC and MF-NPs@F127/F68. Gelation was observed at approximately 32°C for all thickeners, indicating an increase in the viscosity. In addition, we measured the solubility, zeta potential, and membrane permeability of the MF formulation with the thickener, as shown in Table 2. The addition of a thickener to MF-NPs did not significantly change their solubility, and the zeta potentials of MF-NPs@F127/MC and MF-NPs@F127/F68 were similar to those of the MF-NPs without

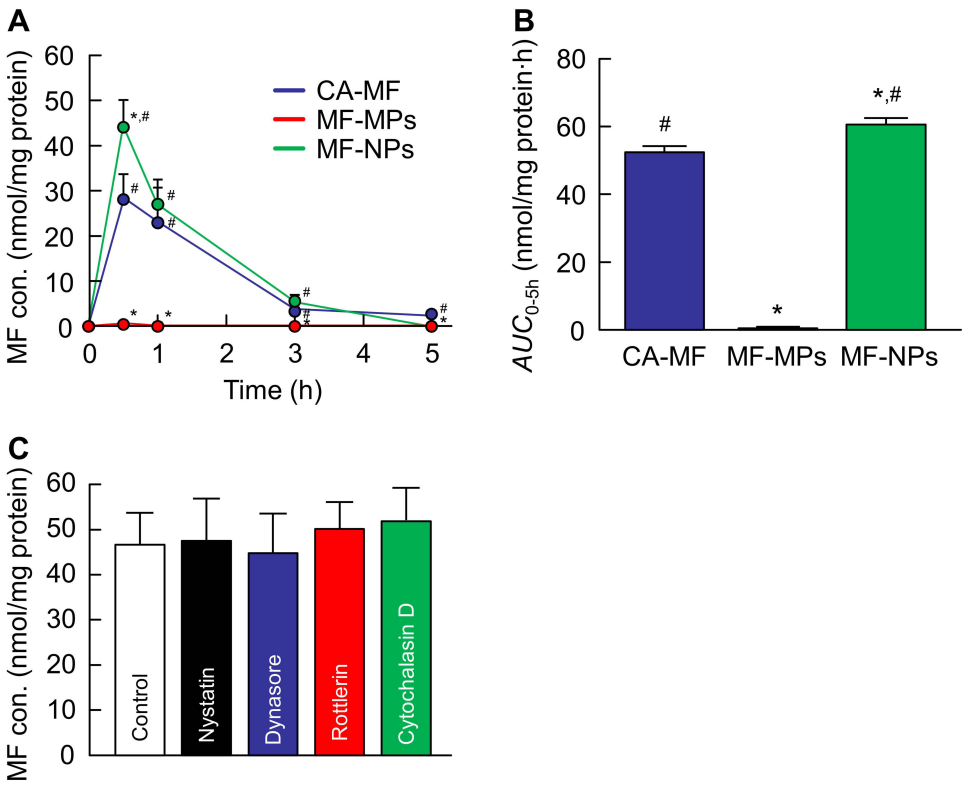

Figure 5 Changes in MF content in nasal mucosa of mice treated with CA-MF, MF-MPs and MF-NPs.

Notes: The Compositions of MF formulations are listed in Table 1. MF content (**A**) and area under the drug concentration–time curve ($AUC_{0\text{-}5h}$) (**B**) in the nasal mucosa after treatment with MF formulations. (**C**) MF content in the nasal mucosa of mice treated with endocytosis inhibitors 30 min after application of MF-NPs. Control: mice treated with dimethyl sulfoxide (DMSO) and MF-NPs. Nystatin: Nystatin-treated mice treated with MF-NPs. Dynasore: Dynasore-treated mice treated with MF-NPs. Rottlerin: rottlerin-treated mice treated with MF-NPs. Cytochalasin D: cytochalasin D-treated mice treated with MF-NPs. n = 5–10 (CA-MF, n=7; MF-MPs, n=8; MF-NPs, n=10; control, n=5; nystatin, n=5; dynasore, n=5; rottlerin, n=5; and cytochalasin D, n=5). *P<0.05 vs CA-MF. #P<0.05 vs MF-MPs.

a thickener. However, the addition of carbopol enhanced negative charge, and the zeta potential of MF-NPs@F127/Car was –83.3 mV. Moreover, the membrane permeability experiment showed that the diffusivity of MF in the MF-NPs decreased with the addition of a thickener (Table 2). Figure 7 shows the changes in nasal absorption of MF-NPs with the addition of thickeners. Contrary to expectations, nasal absorption and duration were reduced by the addition of thickeners, as the MF content in mice treated with MF-NPs@F127/MC, MF-NPs@F127/F68, and MF-NPs@F127/Car was significantly lower than in mice treated with MF-NPs. In particular, the addition of F127/Car strongly attenuated MF delivery to the nasal mucosa compared with MF-NPs@F127/MC and MF-NPs@F127/F68. In this study, we also tried to measure the MF levels in the brain and blood, and no drugs were detected in either group (MF-NPs, MF-NPs@F127/MC, MF-NPs@F127/F68 and MF-NPs@F127/Car).

Discussion

Nasal MF formulation has been shown to significantly reduce both nasal symptoms and improve activity levels and social functioning.[29] In a previous study, administration of nasal MF formulations prior to the pollen season significantly prevented symptoms, and was not associated with serious adverse events.[30] Thus, nasal MF formulation is well tolerated in both children[31] and adults.[30] In this study, we attempted to prepare nanocrystalline MF, and found that the application of nanocrystalline MF in nasal MF formulations would enhance local absorption in comparison with traditional nasal MF formulations. Moreover, we showed that the application of the in situ gelling system attenuated the local absorption of MF-NPs owing to a decrease in drug diffusion in dispersions.

First, dispersions containing nanocrystalline MF were prepared. The bead-milling technique, called the breakdown method, was used to produce nanocrystals in a general study,[19] and highly hydrophobic drugs became meringue-like

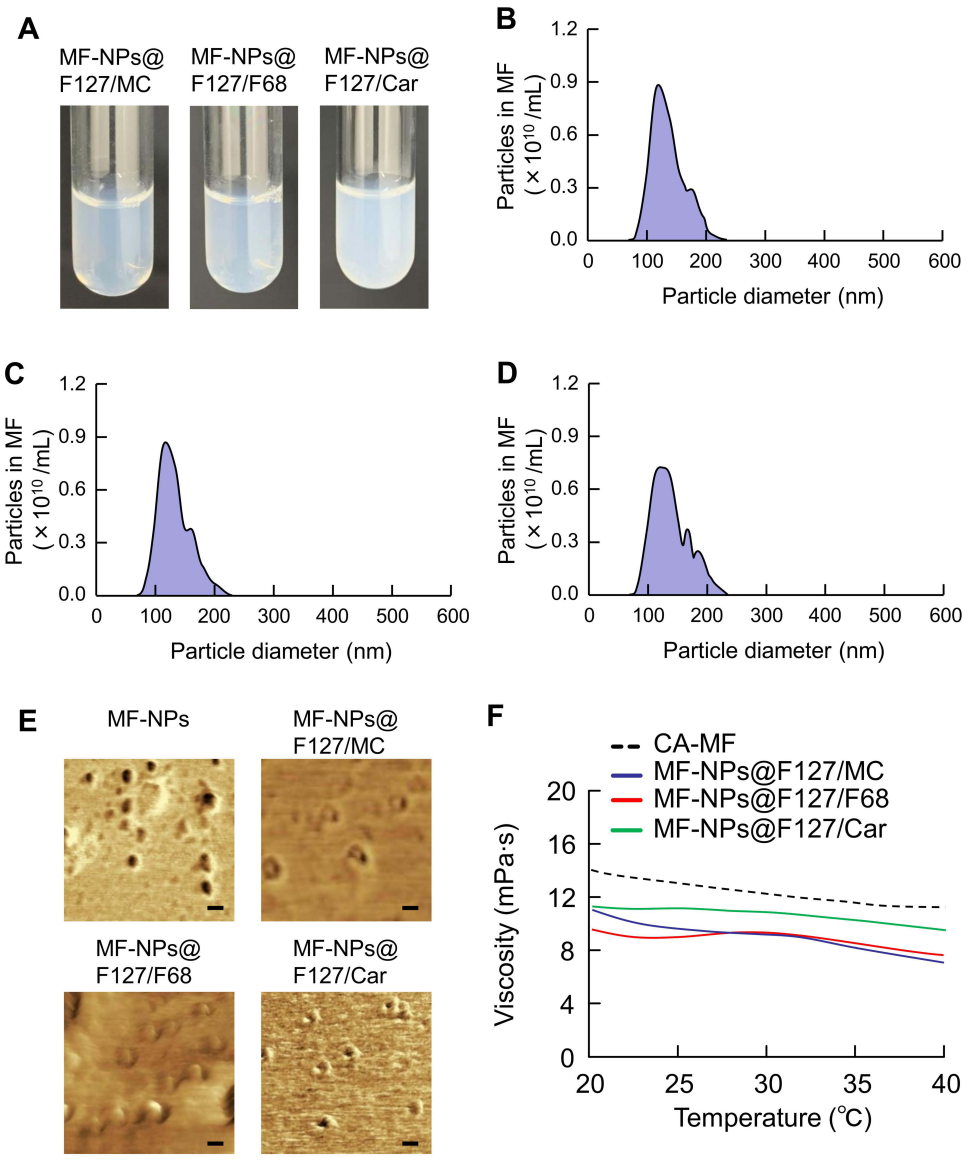

Figure 6 Changes in the particle size and viscosity of MF-NPs by the addition of a thickener.
Notes: The Compositions of MF formulations are listed in Table 1. (**A**)–(**D**) Digital images (**A**) and particle size frequencies of MF-NPs@F127/MC (**B**), MF-NPs@F127/F68 (**C**) and MF-NPs@F127/Car (**D**). (**E**) and (**F**) Scanning probe microscopy (SPM) images (**E**) and viscosities (**F**) of MF-NPs, MF-NPs@F127/MC, MF-NPs@F127/F68, and MF-NPs@F127/Car. Bar in the image (**E**) indicate 100 nm. n = 5.

when subjected to the bead-milling method without MC. Moreover, adsorption to the surface of cyclodextrin decreases the cohesion of nanoparticulate solids.[19] From these previous findings, we used these MC and HPβCD as additives to design MF-NPs. In this study, the MF size in the dispersions was 80–200 nm after bead milling (Figure 1). Second,

Table 2 Particle Sizes, Solubilities, Zeta Potentials, and Membrane Permeabilities of MF Formulations

Formulation	Physical Properties			
	Mean Particle Size (nm)	Solubility (μM)	Zeta Potential (mV)	Membrane Permeability (μM)
MF-MPs	32.6 ± 3.2, ×10^3	21 ± 2.1$^{\#}$	-56.9 ± 3.7	0.32 ± 0.10$^{\#}$
MF-NPs	148.9 ± 2.4*	328 ± 17.4*	-58.8 ± 3.6	2.47 ± 0.29*
MF-NPs@F127/MC	153.1 ± 3.1*	316 ± 18.4*	-53.7 ± 3.6	1.52 ± 0.20*$^{\#}$
MF-NPs@F127/F68	150.9 ± 2.8*	314 ± 18.6*	-58.6 ± 4.2	1.33 ± 0.14*$^{\#}$
MF-NPs@F127/Car	153.5 ± 3.3*	324 ± 21.1*	-83.3 ± 5.1*$^{\#}$	1.16 ± 0.07*$^{\#}$

Notes: Compositions of MF formulations are listed in Table 1. n=7. *P<0.05 vs MF-MPs for each category. $^{\#}P$<0.05 vs MF-NPs for each category.

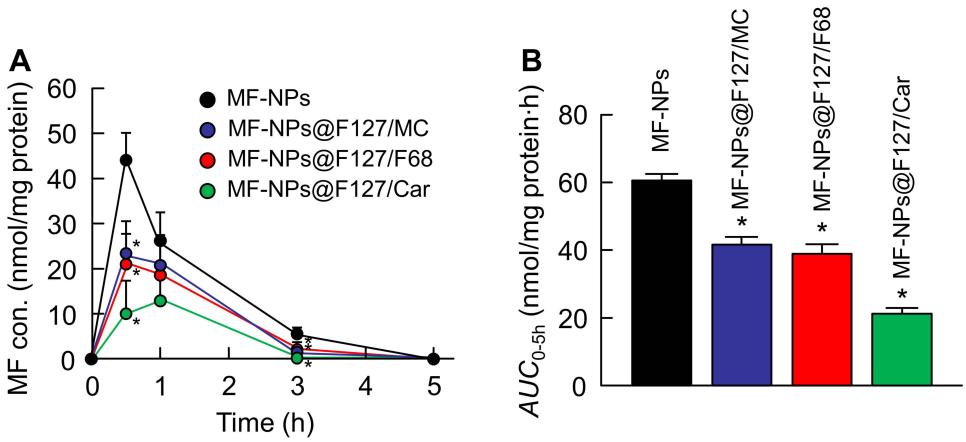

Figure 7 Changes in MF contents (**A**) and $AUC_{0\text{-}5h}$ (**B**) in the nasal mucosa of mice treated with MF-NPs@F127/MC, MF-NPs@F127/F68, and MF-NPs@F127/Car.
Notes: The Compositions of MF formulations are listed in Table 1. n = 6–10 (MF-NPs n=10, MF-NPs@F127/MC n=6, MF-NPs@F127/F68 n=6, MF-NPs@F127/Car n=6). *P<0.05 vs MF-NPs for each category.

thermogravimetry-differential thermal analysis (TG-DTA) and XRD were used to investigate whether the bead-milled MF maintained its crystalline form. The DSC thermogram of raw MF confirmed that endothermic peak between 225–240°C is correlated with the study of Chen et al.[25] The TG-DTA and XRD pattern was not changed in MF with or without bead-milling treatment (Figure 2). These results show that the MF nanoparticles provided in the dispersions with bead milling treatment were nanocrystalline. Subsequently, the characteristics of the MF-NPs were evaluated. If the size of the crystalline drug can be reduced to the nanoscale, as expected from the Ostwald-Freundlich equation, the drug solubility may also improve. The solubility of MF was enhanced by bead milling (Figure 3A). However, excessive miniaturization leads to an increase in the surface energy, which is disadvantageous from the standpoint of the storage stability of the formulation. Therefore, we evaluated the dispersibility of MF-NPs and showed that no aggregation or degradation was observed in the MF-NPs (Figure 3C and D), and the size of the MF particles in the MF-NPs remained nanoscale for 14 days (mean particle size: 158.3 ± 7.3 nm). Otherwise, the dispersibility of CA-MF microparticles (particle size: 0.2–90 μm) was similar to that of MF-NPs (Figure 3). It was known that the viscosity and zeta potential were related to aggregation of dispersions, and the viscosity and negative charge of CA-MF was significantly higher than those of MF-MPs and MF-NPs (Figure 4). These results suggest that these factors contributed to the stable dispersibility of the CA-MF. In addition, it was suggested that the stable dispersibility of MF-NPs may be due to the combination of nanoparticle size and HPβCD, as the dispersibility of MF-NPs without HPβCD was lower than MF-NPs with CD (dispersibility 2 weeks after preparation, 43.3 ± 5.9%, n=3).

Furthermore, it has been reported that the optimal size of nanoparticles (approximately 100 nm) allows for cellular uptake and permeation of the tissue membrane.[18,32–35] Therefore, we demonstrated the drug absorption of MF formulations through the nasal mucosa (Figure 5). The local absorption of MF in mice nasally administered CA-MF and MF-NPs was enhanced in comparison with MF-MPs, and the MF levels in the nasal mucosa of the mice treated with MF-NPs were significantly higher than those in CA-MF 30 min after nasal administration. Moreover, an accumulating evidence demonstrates that drugs deposited in the nasal cavity escape the usual rapid clearance by enzymatic degradation and the mucociliary system, undergo uptake into cells of the olfactory and trigeminal pathways, or are absorbed into the systemic circulation.[36–39] This pathway via the trigeminal pathway can be an important direct pathway for drug delivery to the brain,[38] and this pathway transports only particles of small size (< 200 nm) via a direct passage from the nasal cavity to the brain (passive diffusion).[40] We also measured whether the nasal administration of MF microcrystal dispersions, which is smaller size particles (< 200 nm), delivered to blood and brain in this study. In contrast to the nasal mucosa, the MF is not delivered systemically or to the brain. Previous reports indicate that MF is a drug with relatively low risk of systemic absorption due to its high lipophilicity and low water solubility (20 μM), and that the MF is poorly absorbed into the systemic circulation due to its lipophilicity and extensive first-pass metabolism in the liver,[41] with a reported

bioavailability of <1%.[42] Otherwise, it was reported that the energy-dependent endocytosis is involved in high absorption of drug nanoparticles in the cornea and intestine.[15,17,19] However, the absorption of MF-NFs via energy-dependent endocytosis was also not observed in the nasal mucosa in this study (Figure 5C). These results suggest that energy-dependent endocytosis in the nasal mucosa treated with dispersions containing nanocrystalline MF may be lower than in the corneal and intestinal mucosa. Taken together, we hypothesized that poor aqueous solubility, extensive first-pass metabolism, high lipophilicity, and inactivation of energy-dependent endocytosis are related to low drug delivery to the systemic and brain regions in MF-NPs. In addition, size-derived tissue penetration without energy-dependent endocytosis may be related to the higher absorption of MF-NPs, as local absorption was higher in MF-NPs than in MF-MPs, more so than the difference in solubility. Further studies are required to elucidate the underlying mechanisms.

The absorption and bioavailability of MFs have been extensively studied using various novel strategies including nanocarrier systems, adhesives, and hydrogel- and gel-based systems. Among these, in situ gelation is considered a promising approach for increasing drug residence time in the nasal cavity, reducing efflux through mucociliary clearance of the administered drug, prolonging drug release, and increasing drug absorption.[27,28] Therefore, we investigated the effect of an in situ gel system incorporating MF nanocrystals. Thermo-reversible in situ gels refer to systems that respond to temperature changes and change from solution to gel form in a specific temperature range; polymers that exhibit sol-gel transition in the 28–37°C temperature range prevent transition at room temperature during storage and transport and facilitate rapid sol-gel transition after nasal administration, making nasal gel Pluronic F-127 and Pluronic F-68 are poloxamer forms commonly used in the preparation of nasal formulation.[43] In addition to thermoreversible in situ gel, the pH stimulated gelation was also used as the in situ gel system; carbopol (carbopol 934) is a major pH-responsive agent exhibiting a sol-gel transition at widely varying ambient pH gelation that occurs when the pH is higher than the pKa value of 5.5.[44,45] Upon contact with nasal fluid, such formulations containing carbopol undergo a conformational change, forming a three-dimensional network, leading to sol-gel conversion.[44,45] Because of its excellent adhesive properties, carbopol is widely used in the preparation of gel-based drug carrier systems for nasal, transdermal, buccal, rectal and ocular administration.[46,47] In recent years, polymer combinations have been used in drug delivery systems to reduce the total in situ gel content and improve gelation properties, and several ocular formulations combining Pluronic F-127 with MC (MC/F127), Pluronic F-68 (F68/F127), carbopol (Car/F127) have been reported.[48–54] In this study, we selected the Pluronic F-127, Pluronic F-68 and carbopol as the base of in situ gel, and attempted to prepare the in situ gel system incorporating MF-NPs (MF-NPs@F127/MC, MF-NPs@F127/F68 and MF-NPs@F127/Car are listed in Table 1). The particle sizes of MF-NPs@F127/MC, MF-NPs@F127/F68, and MF-NPs @F127/Car were at the nanoscale, and their solubilities and zeta potentials were similar to those of the MF-NPs (Table 2; Figure 6). In addition, these viscosities were enhanced in comparison with those of the MF-NPs at 20–40°C (Figure 6F). It was expected that the in situ gel system incorporating nanocrystalline MF would enhance local, systemic, and brain delivery through the nose; however, absorption decreased in the three in situ gel formulations (Figure 7). Our previous studies have shown that drug absorption by drug nanocrystal dispersions was prevented as the diffusivity of the nanocrystal phase decreased in the solvent.[20,21,55] Therefore, we measured the diffusivity of nanocrystalline MF in dispersions, and the in situ gel formulations incorporating MF nanocrystals were lower than those of MF-NPs (Table 2; Figure 3B). The decreased diffusivity of the nanocrystal layer may have prevented nasal absorption. The drug particle size of the CA-MF was similar to that of the MF-MPs, the viscosity was higher, and the diffusion was lower than the in situ gel system incorporating nanocrystalline MF, although the drug absorption was higher than of the MF-MPs and in situ gelation incorporating MF nanocrystals (Figures 3, 5, and 7). CA-MF contained benzalkonium chloride, polysorbate 80, crystalline cellulose, sodium carmellose, glycerin, and a pH adjuster (benzalkonium chloride, polysorbate 80, crystalline cellulose, sodium carmellose, CA-MF may pH adjuster) as additives. However, further studies are required to confirm these findings.

Further studies are needed to clarify the detailed mechanism of the transnasal penetration of MF nanocrystals with or without in-situ gelling system. Moreover, it is important to elucidate the effects of the nasal administration of MF-NPs. Therefore, we evaluated the therapeutic effects of MF-NPs on allergic rhinitis using animal models. In addition, we plan to measure in vitro MF penetration using fresh nasal mucosa to mimic in vivo conditions.

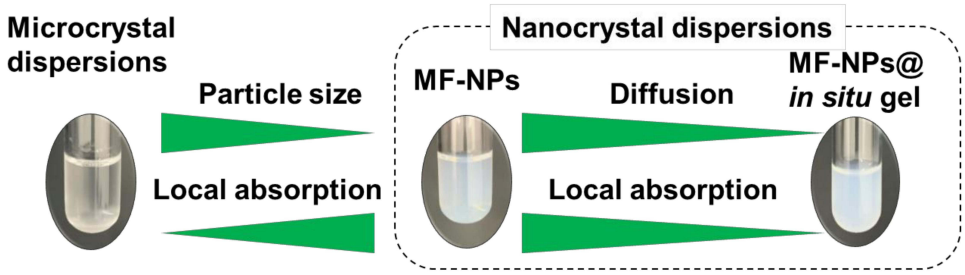

Figure 8 Mechanism for nasal absorption after treatment with MF nanocrystals.

Conclusion

In this study, we successfully prepared MF-NPs with and without an in situ gelling system. We found that nanoparticulation increased the local absorption of MF; (local absorption of MF-NPs was higher than those of CA-MF and MF-MPs) (Figure 8). In addition, this study suggests that, unlike the results observed in the small intestine and corneal tissue, the high absorption of nanocrystalline MF in the nasal mucosa may be related to a pathway that is not derived from energy-dependent endocytosis. Moreover, the application of the in situ gelling system attenuated the local absorption of MF-NPs owing to the decrease in drug diffusion in the dispersions (Figure 8). In contrast to local absorption, MF cannot be delivered systemically or to the brain via nasal administration of MF-NPs. Thus, we found that the nanoparticulation of MF enhances local intranasal bioavailability and that the regulation of viscosity is an important factor in the design of nasal formulations based on MF nanocrystals. These findings provide insights for the design of novel nanomedicines with enhanced nasal bioavailability.

Abbreviations

AUC, area under the drug concentration–time curve; CA-MF, commercially available mometasone furoate; HPβCD, 2-hydroxypropyl-β-cyclodextrin; MC, methylcellulose; MF, mometasone furoate; MF-MPs, mometasone furoate microcrystal dispersions; MF-NPs, mometasone furoate nanocrystal dispersions; MF-NPs@F127/MC, mometasone furoate nanocrystal dispersions containing Pluronic F-127 and methylcellulose; MF-NPs@F127/F68, mometasone furoate nanocrystal dispersions containing Pluronic F-127 and Pluronic F-68; MF-NPs@F127/Car, mometasone furoate nanocrystal dispersions containing Pluronic F-127 and carbopol; SPM, scanning probe microscope; TG-DTA, thermogravimetry-differential thermal analysis; XRD, X-ray diffraction.

Ethics Approval and Consent to Participate

This study was approved by Kindai University on April 1, 2020, with the project identification code KAPS-2020-013. This study was conducted in accordance with ARRIVE guidelines.

Author Contributions

All authors made a significant contribution to the work reported, whether that is in the conception, study design, execution, acquisition of data, analysis and interpretation, or in all these areas; took part in drafting, revising or critically reviewing the article; gave final approval of the version to be published; have agreed on the journal to which the article has been submitted; and agree to be accountable for all aspects of the work.

Disclosure

The authors report no conflicts of interest in this work.

References

1. Prenner BM, Schenkel E. Allergic rhinitis: treatment based on patient profiles. *Am J Med*. 2006;119(3):230–237. doi:10.1016/j.amjmed.2005.06.015
2. Compalati E, Penagos M, Henley K, Canonica GW. Allergy prevalence survey by the World Allergy Organization. *Allergy Clin Immunol Int J World Allergy Org*. 2007;19:82–90.

3. Asher MI, Montefort S, Björkstén B, et al. Worldwide time trends in the prevalence of symptoms of asthma, allergic rhinoconjunctivitis, and eczema in childhood: ISAAC Phases One and Three repeat multicountry cross-sectional surveys. *Lancet*. 2006;368(9537):733–743. doi:10.1016/S0140-6736(06)69283-0
4. van Cauwenberge P, Bachert C, Passalacqua G, et al. Consensus statement on the treatment of allergic rhinitis. European Academy of Allergology and Clinical Immunology. *Allergy*. 2000;55(2):116–134.
5. Bousquet J, van Cauwenberge P, Khaltaev N, et al. Allergic rhinitis and its impact on asthma. *J Allergy Clin Immunol*. 2001;108(5 Suppl):S147–S334.
6. Scadding GK, Durham SR, Mirakian R, et al. BSACI guidelines for the management of allergic and non-allergic rhinitis. *Clin Exp Allergy*. 2008;38(1):19–42.
7. Plaut M, Valentine MD. Clinical practice. Allergic rhinitis. *N Engl J Med*. 2005;353(18):1934–1944. doi:10.1056/NEJMcp044141
8. Prakash A, Benfield P. Topical mometasone. A review of its pharmacological properties and therapeutic use in the treatment of dermatological disorders. *Drugs*. 1998;55(1):145–163. doi:10.2165/00003495-199855010-00009
9. Affrime MB, Cuss F, Padhi D, et al. Bioavailability and metabolism of mometasone furoate following administration by metered-dose and dry-powder inhalers in healthy human volunteers. *J Clin Pharmacol*. 2000;40(11):1227–1236. doi:10.1177/009127000004001107
10. Gudis DA, Cohen NA. Cilia dysfunction. *Otolaryngol Clin North Am*. 2010;43(3):461–472. doi:10.1016/j.otc.2010.02.007
11. Rosen H, Abribat T. The rise and rise of drug delivery. *Nat Rev Drug Discov*. 2005;4(5):381–385. doi:10.1038/nrd1721
12. Roy S. Strategic drug delivery targeted to the brain: a review. *Der Pharmac Sin*. 2012;3(1):76–92.
13. Sanjay D, Mahantil B, Majumder B. Nasal drug delivery: an approach of drug delivery through nasal route. *Der Pharmac Sin*. 2011;2(3):94–106.
14. Patra JK, Das G, Fraceto LF, et al. Nano based drug delivery systems: recent developments and future prospects. *J Nanobiotechnology*. 2018;16(1):71. doi:10.1186/s12951-018-0392-8
15. Otake H, Goto R, Ogata F, et al. Fixed-Combination Eye Drops Based on Fluorometholone Nanoparticles and Bromfenac/Levofloxacin Solution Improve Drug Corneal Penetration. *Int J Nanomedicine*. 2021;16:5343–5356. doi:10.2147/IJN.S317046
16. Nagai N, Iwai Y, Sakamoto A, et al. Drug Delivery System Based On Minoxidil Nanoparticles Promotes Hair Growth In C57BL/6 Mice. *Int J Nanomedicine*. 2019;14:7921–7931. doi:10.2147/IJN.S225496
17. Nagai N, Ogata F, Otake H, Nakazawa Y, Kawasaki N. Energy-dependent endocytosis is responsible for drug transcorneal penetration following the instillation of ophthalmic formulations containing indomethacin nanoparticles. *Int J Nanomedicine*. 2019;14:1213–1227. doi:10.2147/IJN.S196681
18. Nagai N, Ogata F, Otake H, Nakazawa Y, Kawasaki N. Design of a transdermal formulation containing raloxifene nanoparticles for osteoporosis treatment. *Int J Nanomedicine*. 2018;13:5215–5229. doi:10.2147/IJN.S173216
19. Nagai N, Ito Y, Okamoto N, Shimomura Y. A nanoparticle formulation reduces the corneal toxicity of indomethacin eye drops and enhances its corneal permeability. *Toxicology*. 2014;319:53–62. doi:10.1016/j.tox.2014.02.012
20. Minami M, Otake H, Nakazawa Y, et al. Balance of Drug Residence and Diffusion in Lacrimal Fluid Determine Ocular Bioavailability in In Situ Gels Incorporating Tranilast Nanoparticles. *Pharmaceutics*. 2021;13(9):1425. doi:10.3390/pharmaceutics13091425
21. Nagai N, Isaka T, Deguchi S, et al. In Situ Gelling Systems Using Pluronic F127 Enhance Corneal Permeability of Indomethacin Nanocrystals. *Int J Mol Sci*. 2020;21(19):7083. doi:10.3390/ijms21197083
22. Mäger I, Langel K, Lehto T, Eiríksdóttir E, Langel U. The role of endocytosis on the uptake kinetics of luciferin-conjugated cell-penetrating peptides. *Biochim Biophys Acta*. 2012;1818(3):502–511. doi:10.1016/j.bbamem.2011.11.020
23. Malomouzh AI, Mukhitov AR, Proskurina SE, Vyskocil F, Nikolsky EE. The effect of dynasore, a blocker of dynamin-dependent endocytosis, on spontaneous quantal and non-quantal release of acetylcholine in murine neuromuscular junctions. *Dokl Biol Sci*. 2014;459:330–333. doi:10.1134/S0012496614060052
24. Hufnagel H, Hakim P, Lima A, Hollfelder F. Fluid phase endocytosis contributes to transfection of DNA by PEI-25. *Mol Ther*. 2009;17(8):1411–1417. doi:10.1038/mt.2009.121
25. Chen XS, Carillo M, Haltiwanger RC, Bradley P. Solid state characterization of mometasone furoate anhydrous and monohydrate forms. *J Pharm Sci*. 2005;94(11):2496–2509. doi:10.1002/jps.20470
26. Khan AR, Liu M, Khan MW, Zhai G. Progress in brain targeting drug delivery system by nasal route. *J Control Release*. 2017;268:364–389. doi:10.1016/j.jconrel.2017.09.001
27. Aderibigbe BA. In Situ-Based Gels for Nose to Brain Delivery for the Treatment of Neurological Diseases. *Pharmaceutics*. 2018;10(2):40. doi:10.3390/pharmaceutics10020040
28. Karavasili C, Fatouros DG. Smart materials: in situ gel-forming systems for nasal delivery. *Drug Discov Today*. 2016;21(1):157–166. doi:10.1016/j.drudis.2015.10.016
29. Yamada T, Yamamoto H, Kubo S, et al. Efficacy of mometasone furoate nasal spray for nasal symptoms, quality of life, rhinitis-disturbed sleep, and nasal nitric oxide in patients with perennial allergic rhinitis. *Allergy Asthma Proc*. 2012;33(2):e9–16.
30. Pitsios C, Papadopoulos D, Kompoti E, et al. Efficacy and safety of mometasone furoate vs nedocromil sodium as prophylactic treatment for moderate/severe seasonal allergic rhinitis. *Ann Allergy Asthma Immunol*. 2006;96(5):673–678. doi:10.1016/S1081-1206(10)61064-2
31. Meltzer EO, Baena-Cagnani CE, Gates D, Teper A. Relieving nasal congestion in children with seasonal and perennial allergic rhinitis: efficacy and safety studies of mometasone furoate nasal spray. *World Allergy Organ J*. 2013;6(1):5.
32. Nagai N, Ogata F, Yamaguchi M, et al. Combination with l-Menthol Enhances Transdermal Penetration of Indomethacin Solid Nanoparticles. *Int J Mol Sci*. 2019;20(15):3644. doi:10.3390/ijms20153644
33. Cevc G, Vierl U. Nanotechnology and the transdermal route: a state of the art review and critical appraisal. *J Control Release*. 2010;141(3):277–299. doi:10.1016/j.jconrel.2009.10.016
34. Nagai N, Iwamae A, Tanimoto S, Yoshioka C, Ito Y. Pharmacokinetics and Antiinflammatory Effect of a Novel Gel System Containing Ketoprofen Solid Nanoparticles. *Biol Pharm Bull*. 2015;38(12):1918–1924.
35. Nagai N, Ogata F, Ishii M, et al. Involvement of Endocytosis in the Transdermal Penetration Mechanism of Ketoprofen Nanoparticles. *Int J Mol Sci*. 2018;19(7):2138. doi:10.3390/ijms19072138
36. Pardeshi CV, Belgamwar VS. Direct nose to brain drug delivery via integrated nerve pathways bypassing the blood–brain barrier: an excellent platform for brain targeting. *Expert Opin Drug Deliv*. 2013;10(7):957–972. doi:10.1517/17425247.2013.790887
37. Lochhead JJ, Thorne RG. Intranasal delivery of biologics to the central nervous system. *Adv Drug Deliv Rev*. 2012;64(7):614–628.

38. Dhuria SV, Hanson LR, Frey WH. Intranasal delivery to the central nervous system: mechanisms and experimental considerations. *J Pharm Sci*. 2010;99(4):1654–1673.
39. Gizurarson S. Anatomical and histological factors affecting intranasal drug and vaccine delivery. *Curr Drug Deliv*. 2012;9(6):566–582. doi:10.2174/156720112803529828
40. Ahmad E, Feng Y, Qi J, et al. Evidence of nose-to-brain delivery of nanoemulsions: cargoes but not vehicles. *Nanoscale*. 2017;9(3):1174–1183. doi:10.1039/C6NR07581A
41. Brannan MD, Herron JM, Affrime MB. Safety and tolerability of once-daily mometasone furoate aqueous nasal spray in children. *Clin Ther*. 1997;19(6):1330–1339. doi:10.1016/S0149-2918(97)80008-2
42. Passali D, Spinosi MC, Crisanti A, Bellussi LM. Mometasone furoate nasal spray: a systematic review. *Multidiscip Respir Med*. 2016;11:18.
43. Sherafudeen SP, Vasantha PV. Development and evaluation of in situ nasal gel formulations of loratadine. *Res Pharm Sci*. 2015;10(6):466–476.
44. Chassenieux C, Tsitsilianis C. Recent trends in pH/thermo-responsive self-assembling hydrogels: from polyions to peptide-based polymeric gelators. *Soft Matter*. 2016;12(5):1344–1359.
45. Sherje AP, Londhe V. Development and Evaluation of pH-Responsive Cyclodextrin- Based in situ Gel of Paliperidone for Intranasal Delivery. *AAPS PharmSciTech*. 2018;19(1):384–394.
46. Yahagi R, Machida Y, Onishi H. Mucoadhesive suppositories of ramosetron hydrochloride utilizing Carbopol. *Int J Pharm*. 2000;193(2):205–212. doi:10.1016/S0378-5173(99)00338-5
47. Wang X, Liu G, Ma J, et al. In situ gel-forming system: an attractive alternative for nasal drug delivery. *Crit Rev Ther Drug Carrier Syst*. 2013;30(5):411–434. doi:10.1615/CritRevTherDrugCarrierSyst.2013007362
48. Zhang M, Djabourov M, Bourgaux C, Bouchemal K. Nanostructured fluids from pluronic mixtures. *Int J Pharm*. 2013;454(2):599–610.
49. Achouri D, Alhanout K, Piccerelle P, Andrieu V. Recent advances in ocular drug delivery. *Drug Dev Ind Pharm*. 2013;39(11):1599–1617. doi:10.3109/03639045.2012.736515
50. Almeida H, Amaral MH, Lobão P, Sousa Lobo JM. Applications of poloxamers in ophthalmic pharmaceutical formulations: an overview. *Expert Opin Drug Deliv*. 2013;10(9):1223–1237. doi:10.1517/17425247.2013.796360
51. El-Kamel AH. In vitro and in vivo evaluation of Pluronic F127-based ocular delivery system for timolol maleate. *Int J Pharm*. 2002;241(1):47–55.
52. Almeida H, Amaral MH, Lobão P, Sousa Lobo JM. In situ gelling systems: a strategy to improve the bioavailability of ophthalmic pharmaceutical formulations. *Drug Discov Today*. 2014;19(4):400–412.
53. Khateb KA, Ozhmukharnetova EK, Mussin MN, et al. In situ gelling systems based on Pluronic F127/Pluronic F68 formulations for ocular drug delivery. *Int J Pharm*. 2016;502(1–2):70–79. doi:10.1016/j.ijpharm.2016.02.027
54. Lin HR, Sung KC. Carbopol/pluronic phase change solutions for ophthalmic drug delivery. *J Control Release*. 2000;69(3):379–388.
55. Nagai N, Minami M, Deguchi S, Otake H, Sasaki H, Yamamoto N. An in situ Gelling System Based on Methylcellulose and Tranilast Solid Nanoparticles Enhances Ocular Residence Time and Drug Absorption Into the Cornea and Conjunctiva. *Front Bioeng Biotechnol*. 2020;8:764. doi:10.3389/fbioe.2020.00764